Chapter 4:

Studies of Palladium Schiff-base Complexes Encapsulated in Zeolite Y and their Catalytic Activity for the Sulfoxidation Reaction

4.1. INTRODUCTION

The selective oxidation of thio-ethers is a significant reaction in organic synthesis,[1] since the product sulfoxides is the important intermediate of various biological advances in natural compounds.[2, 3] These products also have versatile applications in agrochemical,[4, 5] pharmaceutical,[6] polymer[7] industries and also can be used as ligands in asymmetric catalysis,[8] oxo-transfer reagents and solvents.[6] They often play an important role as therapeutic agents such as anti-ulcer,[9, 10] antibacterial, antifungal, anti-atherosclerotic,[11, 12] anthelmintic,[13] antihypertensive, [14] and vasodilators.[15] As a result, there are substantial amount of work has been done to develop varieties of competent catalysts for the sulfoxidation process.[16-27] Most of conventional synthetic routes for sulfoxidation process are quite efficient but they require the use of lots of organic and inorganic oxidants, solvents which obviously leads to produce a large amount of toxic waste.[28, 29] Consequentially, it is essential to develop the 'greener approach' to get the desired sulfoxidation products. In order to adopt the environment benign methodology there should be some modification in traditional the procedures like uses of environment friendly oxidants, solvent free reaction medium and eco-friendly catalysts. Aqueous hydrogen peroxide is most popular oxidant for the sulfoxidation process because of easy handling, greater availability, and eco friendly approach for the reaction due to formation of water as the only by-product.[23] Schiff base transition metal complexes have played vital role for the progress of catalytic processes with greater utility in biological and industrial applications.[30-33] However the homogeneous catalysts generally have some disadvantages in the catalytic processes like, their instability, difficulty in the separation, lack of reusability and lack of greener approach.[34-36]. The modern catalytic science favors those catalysts, which can conquer the limitation of these homogeneous catalysts without loss of reactivity. In this direction, heterogenisation of conventional homogeneous catalyst is a suitable route to couple the reactivity of the complex with the additional shape and size-selectivity and site isolation properties appended by the host materials. Encapsulation of transition metal complexes in different host like microporus, mesoporous materials is an alternative contemporary approach to accomplish the synthesis of designer catalyst.[37-42] In this order, zeolites are found as competent hosts for the synthesis of so-called biomimetic systems by encapsulating those transition metal complexes which are having comparable molecular dimension with that of cavity of the host zeolites.[39, 43] Among

those, employment of zeolite encapsulated metal complexes in the field of oxidation or epoxidation of alkanes, alkenes, alcohols and aromatic compounds by zeolite encapsulated metal complexes have been extensively studied and reported ,[38, 40, 44-51] but comparatively lesser reports are available on sulfoxidation process.[52-56] Maurya and co-workers have investigated different vanadium complexes entrapped in zeolite Y and explored their catalytic activities for the oxidation and sulfoxidation reaction.[52-55] The authors have stated that the encapsulated complexes in zeolite Y have shown almost similar reactivity for the sulfoxidation reaction when compared with their free states. However, higher turnover frequencies and reusability make the zeolite-encapsulated complexes more suitable than their free state analogues.

In present work, we have synthesized some novel palladium Schiff-base complexes in encapsulated state in zeolite Y as well as in free states. The molecular dimensions of complexes followed the order as PdL1<PdL3<PdL4<PdL5<PdL6. These systems are employed as catalysts for the sulfoxidation of methyl phenyl sulfide to study the steric and electronic effect of different substituent's groups which are attached on the complexes, and their consequences on the reactivity upon encapsulation. These systems are well characterized by powder XRD, XPS, SEM-EDS, IR and UV-Visible spectroscopy. It is quite fascinating to observe that as compared to the neat complexes, encapsulated complexes are much better catalysts for the conversion of methyl phenyl sulfide to corresponding sulfoxide and interestingly, reactivity of encapsulated systems are largely controlled by the extent of space constraint imposed by the host framework of zeolite Y.

4.2. RESULTS AND DICUSSION

The synthesis of Schiff-base ligands (L1, L3, L4, L5 and L6) and free state palladium Schiff-base complex (PdL1, PdL3, PdL4, Pd L5 and PdL6) have already been discussed in chapter 2 (experimental section).

4.2.1. Elemental Analysis

The pure Na-zeolite Y has the unit cell formula as $Na_{58}Al_{58}Si_{136}O_{388}{\bullet}yH_2O$ and Si/Al ratio is 2.34. The elemental analysis (EDS spectra) of encapsulated complexes PdL1, PdL3, PdL4, PdL5, and PdL6, have suggested that Si/Al ratio remains unaffected even after the encapsulation for all the cases (Appendix A18-A23) indicating that the dealumination doesn't

take place during the process of encapsulation. The concentration of palladium metal ion in the Pd-exchanged zeolite and encapsulated metal complexes in wt% given in table 4.1 indicates the concentration of palladium metal ions in Pd-exchanged zeolite Y is greater than that of the all the zeolite encapsulated complexes. It is quite reasonable because in the process of encapsulation slight leaching of metal ions may occur which eventually leads to the reduction of the wt% of palladium in encapsulated metal complexes.

Table 4.1: Concentration of palladium (wt %) content in the different samples.

S.No	Samples	Palladium (wt %)	Si/Al ratio
1.	Parent Y	-	2.90
2.	Pd-Y	0.65	2.79
3.	PdL1-Y	0.51	2.85
4.	PdL3-Y	0.27	2.89
5.	PdL4-Y	0.27	1.28
6.	PdL5-Y	0.26	2.78
7.	PdL6-Y	0.22	2.79

4.2.2. Scanning Electron Microscopy

Scanning electron microscopic studies of pure zeolite Y and the Soxhlet extracted hybrid PdL1-Y, PdL3-Y, PdL4-Y, PdL5-Y, and PdL6-Y systems are carried out (SEM images are shown in Figure 4.1). Complex formation is required only inside the cavities but practically it is not viable, because some of the metal complexes can always be adsorbed on surface or some ligands may remain uncoordinated. To investigate surface morphology of zeolite Y specifically after encapsulation SEM images before or after Soxhlet extraction are taken, After Soxhlet extraction, zeolite boundaries are evidently observable in the SEM images of zeolite entrapped complexes and also comparable with that of the pure zeolite Y. This manifests the absence of unreacted species or impurities on the surface of host lattice in the

final host-guest products.[57, 58] The color of Soxhlet extracted final product definitely is a sign of successful encapsulation of the complex inside the cavities of zeolite.

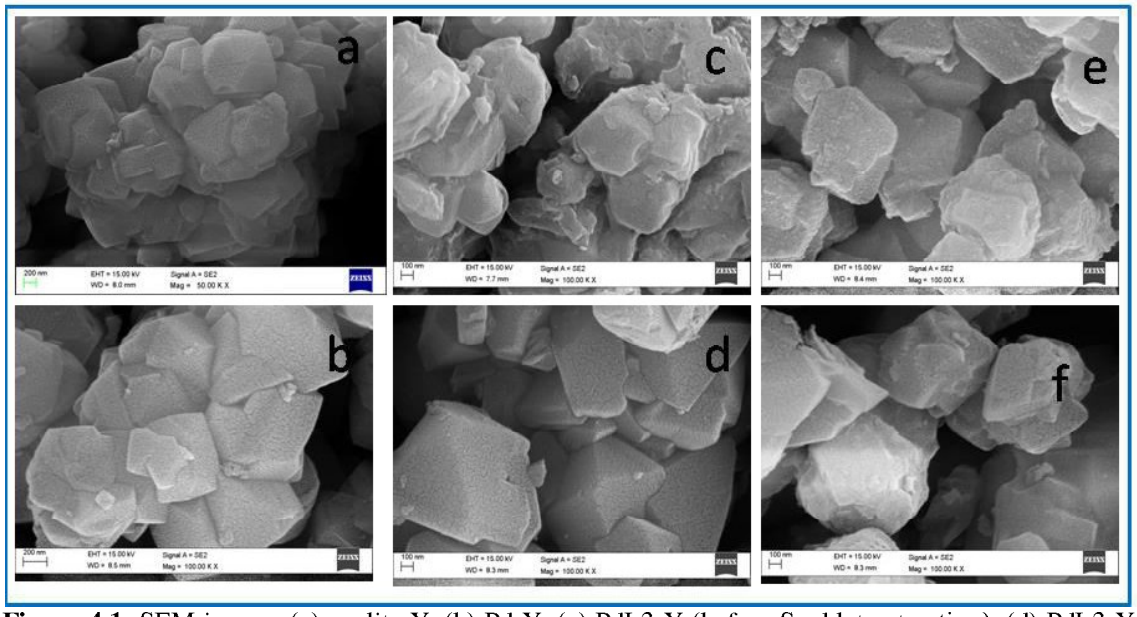

Figure 4.1: SEM images (a) zeolite Y, (b) Pd-Y, (c) PdL3-Y (before Soxhlet extraction) (d) PdL3-Y (after Soxhlet extraction), (e) PdL4-Y, (f) PdL6-Y.

4.2.3. Powder X-ray Diffraction Analysis

Powder X-ray diffraction patterns of parent zeolite Y, Pd-zeolite-Y and palladium salen complexes encapsulated in zeolite Y have been recorded (Given in Figure 4.2). The complexes are systhesized within the supercage of zeolite Y *via* flexible ligand synthesis method and the unreacted ligands and complexes are completely removed by Soxhlet extraction however during the whole process the host framework is remained intact. The X-ray diffractograms of PdL1-Y, PdL3-Y, PdL4-Y, PdL5-Y and PdL6-Y samples and that of the pure zeolite Y, exhibit no shift in peak positions when compared. This observation is indeed a significant one as it specifies the preservation of host lattice intigrity even after the encapsulation of a large complex into it. However, XRD patterns of PdL1-Y, PdL3-Y, PdL4-Y, PdL5-Y and PdL6-Y evidently illustrate a substantial reversal in the intensity of the peaks at $2\theta=10°$ and 12° i.e., ($I_{220} < I_{311}$) in comparison to that in the XRD patterns of pure and Pd-exchanged zeolite Y. This intensity reversal has already been empirically correlated with the existence of the large complex inside the cavity of zeolite Y.[59, 60] Interestingly, tethered complex on the host surface doesn't show such type of intensity reversal in XRD patterns.

Moreover, the absence of new peaks in XRD patterns of palladium encapsulated complexes is a signature of formation of the complexes in low concentrations inside the host lattice.

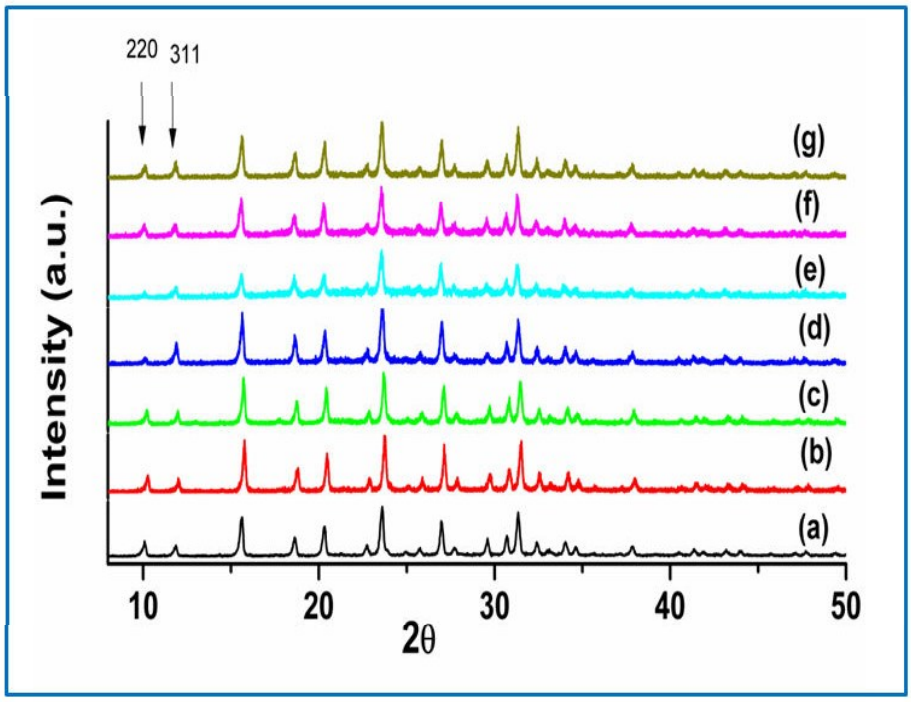

Figure 4.2: XRD pattern of (a) Pure zeolite-Y, (b) Pd-exchanged zeolite -Y, (c) PdL1-Y, (d) PdL3-Y, (e) PdL4-Y, (f) PdL5-Y, and (g) PdL6-Y.

4.2.4. X-Ray Photoelectron Spectroscopy (XPS)

X-ray photoelectron spectroscopy (XPS) is an important technique which provides the indirect proof of the complex formation in free as well as encapsulated state. All core constituent elements of the complexes like C (1s), N (1s), O (1s) and Pd (3d) of PdL1, PdL1-Y, PdL3-Y and PdL6-Y complexes are presented in the form of survey spectra and high resolution spectra in Figure 4.3-4.6 and corresponding binding energy data are tabulated in Table 4.2. The obsrved data evidently indicate the presence of C, N, O, Na, Si, Al and Pd in their respective chemical states, which are in accordance to the literature.[40, 61-65] Intense and broad carbon (1s) XPS spectra have been observed for palladium salen complexes in both states and are further deconvoluted into two peaks and confirmed the presence of sp^3 and sp^2 carbon atoms in those complexes. Similarly these complexes have shown the XPS signals for nitrogen (1s), oxygen (1s), and validated for the (M-N), (N=C) and (C-O), (M-O) elemental state respectively. All the encapsulated complexes show very weak signal for palladium

metal because of its low loading level within the host lattice. High resolution XPS spectra of palladium in PdL1 complex has shown two signals at the binding energies 335.96 and 340.96 eV which are attributed to $3d_{5/2}$ and $3d_{3/2}$ respectively. However, when the complex is encapsulated in zeolite Y, $3d_{5/2}$ and $3d_{3/2}$ XPS signals are broader and appear on the almost same binding energies (335.13, 340.49 eV), additionally a new signal originates at relatively higher binding energy of 347.87 eV. This additional XPS signal at higher binding energy has been observed for all the encapsulated complexes (PdL1-Y, PdL3-Yand PdL6-Y) but not for the free state complex (PdL1). Higher shift in binding energy is definitely a consequence of the removal of electron density from the metal center.[40, 65] In this context, it could have relevant significance as the geometry which the metal complex adopts under encapsulation, might play the major role in the depletion of electron density from the metal center. Furthermore, Na (1s), Si (2p) and Al (2p) elements XPS signals are also observed at their expected position in the XPS spectra of all encapsulated complexes.

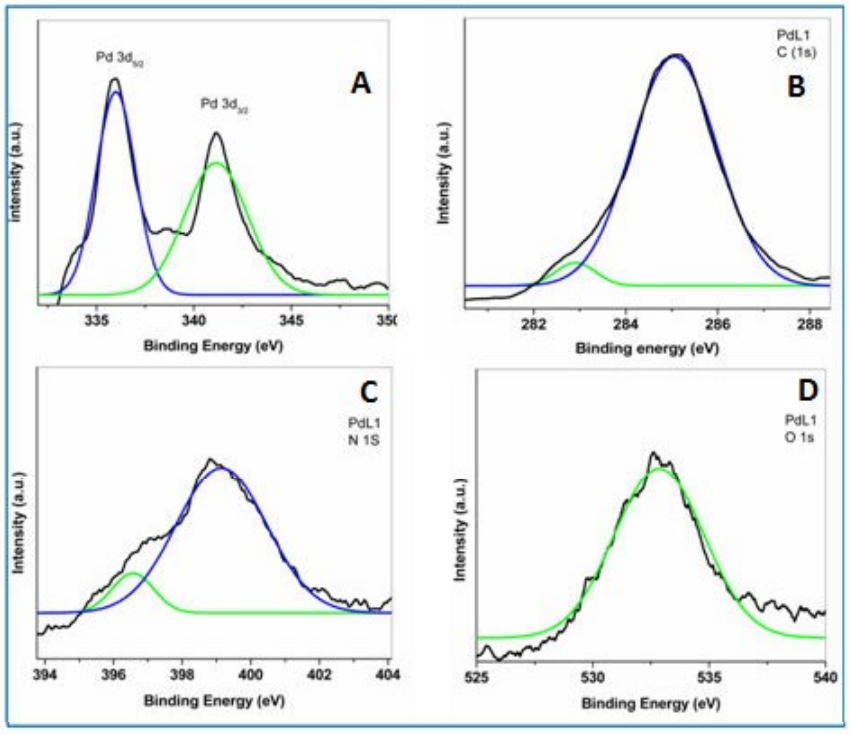

Figure 4.3: High resolution XPS signals of (A) Pd (3d), (B) C (1s), (C) N (1s) and (D) O (1s) for PdL1 Complex. (Black colored graphs are experimental data and green and blue colored peaks are peak fitted data)

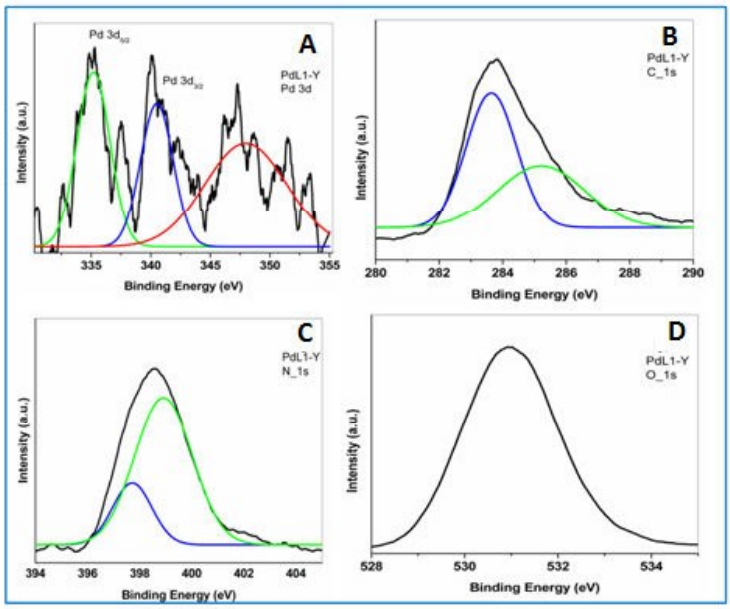

Figure 4.4: High resolution XPS signals of (A) Pd (3d), (B) C (1s), (C) N (1s) and (D) O (1s) for PdL1-Y Complex. (Black colored graphs are experimental data and green and blue colored peaks are peak fitted data)

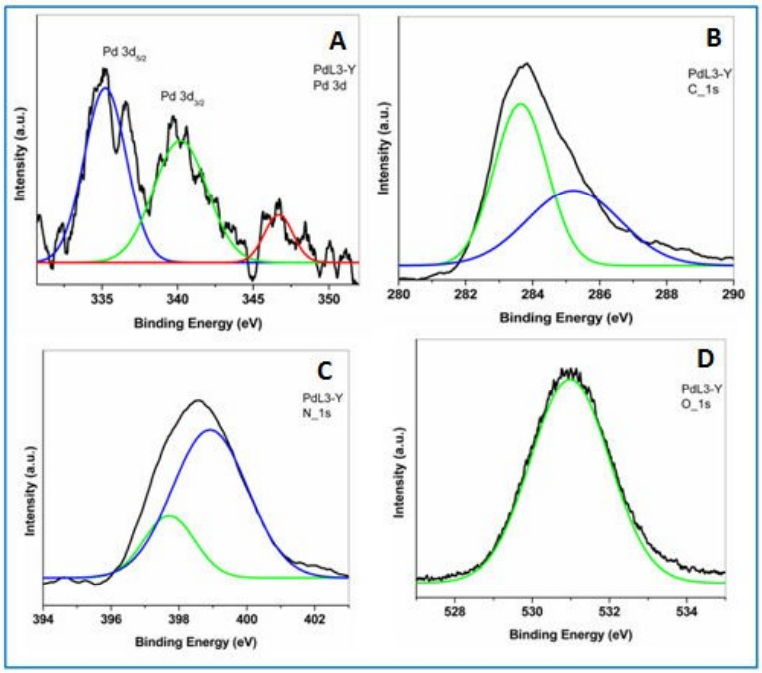

Figure 4.5: High resolution XPS signals of (a) Pd (3d), (b) C (1s), (c) N (1s) and (d) O (1s) for PdL3-Y Complex. (Black colored graphs are experimental data and green and blue colored peaks are peak fitted data)

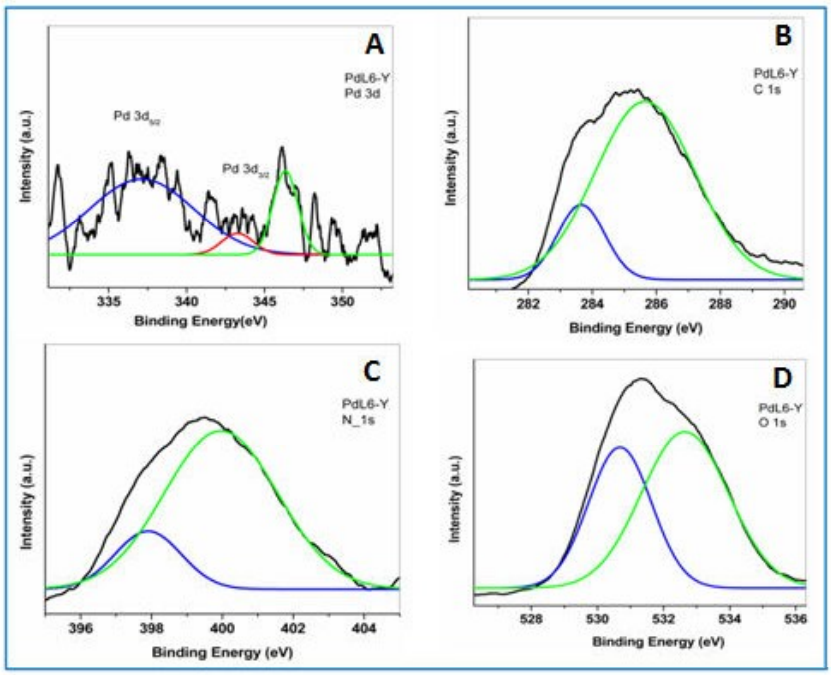

Figure 4.6:. High resolution XPS signals of (A) Pd (3d), (B) C (1s), (C) N (1s) and (D) O (1s) for PdL6-Y Complex. (Black colored graphs are experimental data and green and blue colored peaks are peak fitted data)

Table 4.2: The binding energy data of the free state or encapsulated complexes.

S. No	Sample	Si (2p)	Al (2p)	C (1s)	N(1s)	O (1s)	Pd ($3d_{5/2}$)	Pd ($3d_{3/2}$)
1.	PdL1	-	-	284.04, 282.82	399.11, 396.54	532.84,	335.92,	340.96.
2.	PdL1-Y	101.52	75.15	285.23, 283.65	398.88, 397.72	530.96	335.13,	340.49, 347.87
3.	PdL3-Y	101.55	72.94, 73.79	285.23, 283.65	398.81, 397.76	530.95	335.39,	340.21. 346.72
4.	PdL6-Y	102.72	73.16. 75.47	285.66, 283.64	399.93, 397.88	532.63, 530.69	337.11,	343.34, 346.64

4.2.5. IR Spectroscopy

FT-IR spectral data of ligands, palladium Schiff base complexes in neat as well as encapsulated state along with the pure zeolite Y have been recorded (Figure 4.7, Table 4.3). IR spectroscopic data has provided information about the retention of integrity of zeolite Y framework and also indicated the successful complex formation within the supercage of zeolite Y. The four major zeolitic IR bands are observed in the region of (450-1200) cm^{-1} and two additional peaks have appeared at 1643 cm^{-1} and 3500 cm^{-1}. The IR bands at 560, 717, 786, and 1018 cm^{-1} are attributed as $(Si/Al\text{-}O)_4$ bending mode, double ring, symmetric stretching and asymmetric stretching vibration respectively,[66] whereas IR bands at 3500 cm^{-1} and 1643 cm^{-1} are assigned to surface hydroxylic group and lattice water molecules respectively.[57] All these bands mostly remain unaffected for all these encapsulated systems (PdL1-Y, PdL3-Y, PdL4-Y, PdL5-Y and PdL6-Y), since the host framework doesn't experience any structural modifications during the encapsulation process.

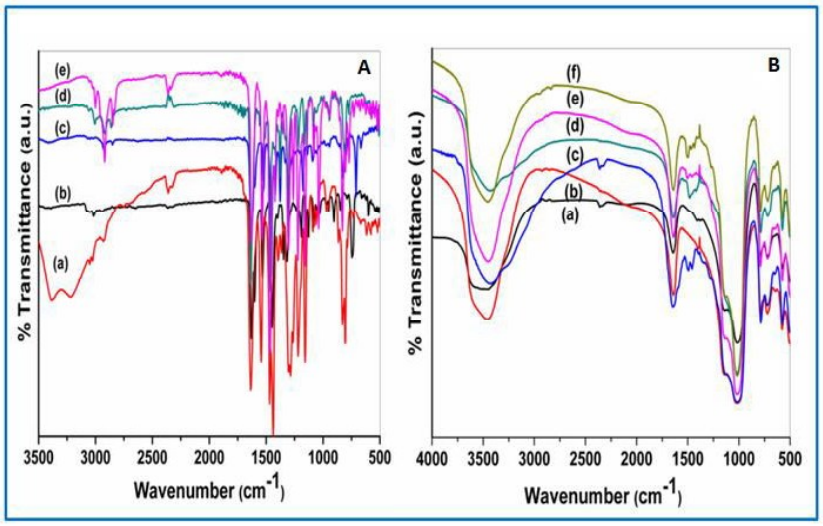

Figure 4.7: (A) FTIR spectra of free state palladium salen complexes (a) PdL1, (b) PdL3, (c) PdL4, (d) PdL5, and (e) PdL6. (B) FTIR spectra of encapsulated palladium salen complexes in zeolite Y (a) Pure zeolite Y, (b) PdL1-Y, (c) PdL3-Y, (d) PdL4-Y, (e) PdL5-Y and (f) PdL6-Y.

However, the salen ligands and corresponding complexes are primarily identified by the IR studies as C=N stretching, C=C stretching and C-O stretching vibrations of the salen ligands appear at the expected positions. Upon complexation these FTIR bands show essentially identical vibration with shifts to lower energies as a outcome of the coordination with the

metal ion. IR peaks of the encapsulated complexes are mostly difficult to identify, because of the appearance of the strong zeolitic bands in the (450–3500) cm^{-1} region. Advantageously, some characteristic IR peaks of relatively low intensities are observed in the range of (1600-1200) cm^{-1} which is mainly due to the guest complex and suitable to study, because zeolitic IR bands are silent particularly in this region. These bands in encapsulated complexes have appeared with little shifts with respect to that of the free state complex, which definitely could be attributed to presence in the different environment. Furthermore, shift in C-H deformation bands has already identified as an indication of encapsulation of the complex inside the zeolite Y.[67]

Table 4.3: FTIR spectral data (in cm^{-1}) for neat and encapsulated state complexes.

S.No	Samples	C=N stretching	C=C stretching	ν_{C-H} deformation	C-O stretching
1.	L1	1633	1557, 1488	1374	1286
2.	PdL1	1632	1531,1447	1346	1219
3.	PdL1-Y	1639	1456	1393	Merged with zeolite band
4.	L3	1639	1508,1454	1385	1257
5.	PdL3	1636	1543, 1439	1393	1219
6.	PdL3-Y	1647	1493, 1458	1396	Merged with zeolite band
7.	L4	1633	1572, 1481	1390	1361
8.	PdL4	1630	1524,1454	1366	1308
9.	PdL4-Y	1640	1537, 1482	1369	1304
10.	L5	1639	1582,1489	1366	1284
11.	PdL5	1634	1531, 1470	1377	1215
12.	PdL5-Y	1634	1506, 1465	1396	Merged with zeolite band
13.	L6	1639	1589,1494	1325	1272
14.	PdL6	1632	1535, 1466	1396	1219
15.	PdL6-Y	1639	1539,1468	1398	1271

4.2.6. Solid state UV-Visible Spectroscopy

Electronic spectra of the ligands and corresponding complexes in solution or solid states have been studied for the justification of complex formation. In addition to that, comparative optical spectra of palladium schiff-base complexes in both states have been studied thoroughly to understand the nature of the geometry they adopt under encapsulation. (Given in Figure 4.8-4.10, Table 4.4). Electronic transition of the Schiff base ligands are appearing in the range of (240-260) nm is assigned as the π–π^* transition and in the range of (320-350) nm as the n–π^* transition. However, in the free state transition metal complexes these transitions are shifted relatively towards lower energy; π–π^* transition have been observed in the range of (224-235) nm and the n–π^* transition in the range of (255-366) nm. The strong evidence of free state complex formation is the appearance of charge transfer (CT) and d–d transitions bands, which are clearly observed in the solid state electronic spectrum in the range of (335-450) nm for different palladium Schiff-base complexes. However, the appearance of d-d bands in square planar palladium complexes is indistinguishable in comparison with that of nickel salen complexes. In palladium salen complexes these bands appear in (335-450) nm region whereas in nickel complexes these are identified in (510-570) nm region. According to ligand field theory, for 4d series element, d orbital splitting is higher quite a large extent as compared to the corresponding 3d series element and due to so, d-d bands in palladium salen complexes have shifted towards high energy region and emerged with charge transfer bands. After encapsulation, palladium salen complexes have shown comparable pattern, however the charge transfer (CT) and d-d bands which are instigated from the metal center are primarily affected i.e., intensified[68] and blue shifted on encapsulation (Similar behavior of nickel Schiff-base complexes are also discussed in chapter 3A, 3B and 3C). Exceptionally different behavior is observed for palladium complexes as PdL4-Y and PdL6-Y have shown additional weak bands in the region of 465 nm and 470 nm respectively. Such behavior of the guest complexes eventually signifies the alteration of the geometry of the complexes especially around the metal center under encapsulation. Interestingly, PdL3-Y, PdL4-Y, PdL5-Y and PdL6-Y complexes have shown the blue shift in greater extent as compared to that observed for PdL1-Y, since these complexes have larger molecular dimension and might experience more space constraint imposed by the topology of the supercage which in turn causes more distortion in the geometry of the complexes.

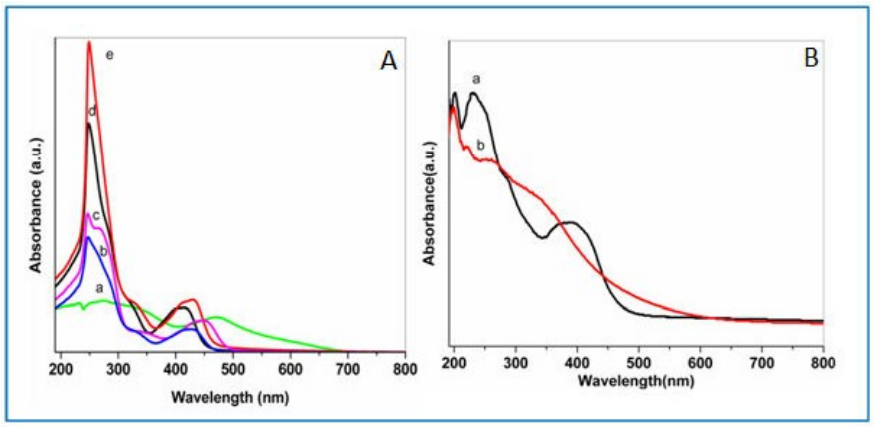

Figure 4.8: (A) **UV**-Vis spectra of free state complexes in chloroform, (a) PdL3, (b) PdL5, (c) PdL6 (d) PdL1 and (e) PdL4. (B).Solid state UV-Vis spectra of (a) PdL1 and (b) PdL1-Y.

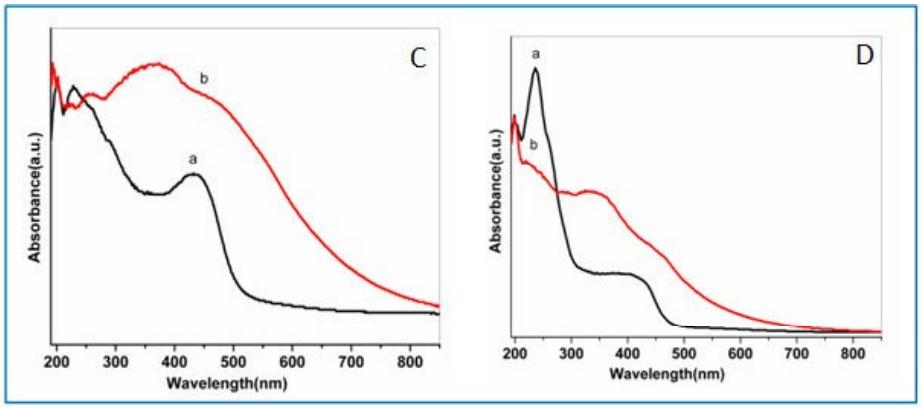

Figure 4.9: **(C)** Solid state UV-Vis spectra of (a) PdL3 and (b) PdL3-Y. (D) Solid state UV-Vis spectra of (a) PdL4 and (b) PdL4-Y.

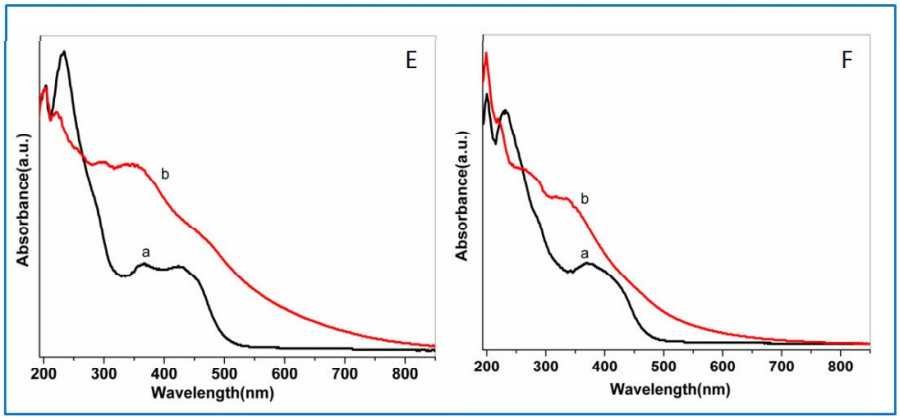

Figure 4.10: **(E)** Solid state UV-Vis spectra of (a) PdL5 and (b) PdL5-Y. (F) Solid state UV-Vis spectra of (a) PdL6 and (b) PdL6-Y.

Table 4.4: Solid state UV-Visible data (in nm) of palladium Schiff-base complexes in both states.

S.No	samples	π—π^* transitions	n—π^* transitions	CT / d-d transitions
1	PdL1	224	255	380-415
2	PdL1-Y	222	262	350-370
3	PdL3	231	261, 296	424-447
4	PdL3-Y	225	255	364, 479
5	PdL4	235	261	404-433
6	PdL4-Y	220	247	323-364, 465
7	PdL5	231	288	372-415
8	PdL5-Y	217	278	335-357
9	PdL6	235	288, 366	435-445
10	PdL6-Y	224	259, 299	346-366, 470

4.2.7. Catalytic Study

Sulfoxidation reaction is effectively catalyzed by transition metal complexes using aqueous hydrogen peroxide.[69] To investigate the effect of geometry of the complexes on their catalytic activity, sulfoxidation reaction has been explored by using H_2O_2 as oxidant under the aerobic condition where both in free and encapsulated states of palladium Schiff-base complexes are employed as catalysts. For all cases methyl phenyl sulfide is converted into corresponding sulfoxide selectively (scheme for sulfoxidation reaction is given in chapter 2 under section 2.2.9). Zeolite encapsulated palladium Schiff-base complexes are comparatively less investigated catalysts for sulfoxidation than the other transition metal-complexes and it is quite interesting to note that the catalytic activities of these encapsulated complexes for the oxidation of methyl phenyl sulfide, in terms of percentage conversion as well as turn over number (TON) are significantly higher than their corresponding free state (Table 4.5, GC chromatograms are shown in Appendix A24-A34).

The modified reactivity of the encapsulated complexes is indeed a consequence of the distorted geometry of the complexes, which they adopt under encapsulation in zeolite Y. It is

quite apparent that these complexes suffer significant distortion due to rigid spherical walls of rigid host zeolite supercage. Distortion in geometry of complex majorly affects the metal center of the complex which is visible in the comparative XPS and optical spectra of the complexes in both the states. Observed relative shifts towards higher value of binding energy in XPS signals for the zeolite encapsulated complexes indicate the enhancement of the electropositive character of the metal center after encapsulation. Such lowering of electron density makes metal center more receptive for the nucleophilic attack. It has been already reported that an electron withdrawing group (Cl^-) makes the copper salen complex distorted from square planar geometry,[70] whereas an electron donating group ($-OCH_3$) on the same position tries to maintain the planarity of the complex. Distortion makes the complex more susceptible for nucleophilic attack by removing electron density from the metal center, on contrary; the metal center of planar conjugated system is electron rich and less efficient for the nucleophilic attacks. We have observed similar effect for the nickel salen complexes, which are having different molecular dimensions.

In the present work, palladium salen complexes have shown similar behavior for the sulfoxidation reaction of methyl phenyl sulfide. Electron withdrawing (-Br groups) in PdL4 makes the complex distorted even in the free state and more reactive for the catalytic process. Electron releasing groups (-OH, and $-OCH_3$) make the palladium salen (PdL3 and PdL6) less reactive for the sulfoxidation process. PdL1 and even PdL5 complexes have exhibited intermediate reactivity as they do not have noteworthy push-pull effect of substituent. As expected, PdL6-Y complex has shown enhanced modified reactivity after encapsulation, the complex is most distorted due to largest molecular dimensions. Theoretical study also supports this fact that after encapsulation the central metal atom of complex may have the more electropositive characters in comparison to its free state. The transition state, as a result becomes more stable, so that electron rich nucleophile is bonded through the axial position.[70] In conclusion it can be stated that the reactivity of free state complexes is mainly governed by the electronic factor and the palladium complexes follow the order as PdL4>PdL1=PdL5>PdL3>PdL6, whereas after encapsulation the catalytic activity order of complexes is in accordance with the molecular dimensions or extent of distortion (PdL6>PdL5>PdL4>PdL3>PdL1).

Table 4.5: Oxidation of methyl phenyl sulfide after 4 hours reaction time with H_2O_2 as oxidant.

S. No	Samples	% Conversion	TON	Selectivity for Sulf	Selectivity for sulfone
1	PdL1	39	30	98.66	1.33
2	PdL1-Y	48	201	97.25	2.74
3	PdL3	30	25	99.51	0.49
4	PdL3-Y	60	477	98.95	1.04
5	PdL4	63	67	98.98	1.01
6	PdL4-Y	71	564	95.45	4.54
7	PdL5	36	30	98.31	1.68
8	PdL5-Y	76	623	92.01	7.98
9	PdL6	26	23	98.18	1.81
10	PdL6-Y	86	835	92.23	7.76

4.3. CONCLUSION

Zeolite encapsulated complexes are indeed better heterogeneous catalysts with enhanced adapted reactivity for the oxidation process. The comparative studies of palladium Schiff-base complexes in free as well as in encapsulated states provide a clear insight about the modified reactivity for the catalytic oxidation processes of such systems after encapsulation. Observed blue shift in d-d bands in the electronic spectra of encapsulated complexes has demonstrated the interference of the space restrictions imposed by rigid host frameworks on the co-ordination environment around the metal because space restrictions compel the encapsulated guest complex to adopt unusual geometry for the accommodation inside the supercage cavity. XPS high resolution spectra of Pd (3d) of encapsulated complexes showing the additional signal towards higher binding energy also confirms the change in the electronic

environment around the metal upon encapsulation. Comparative catalytic studies of these hybrid systems provide a fascinating co-relation between modified structural aspects with adapted functionality of complexes and can be concluded as the degree of distortion in the structure of the encapsulated complex is the key point for the remarkable modified catalytic activity of the systems.

REFERENCES

1. M. Madesclaire, *Tetrahedron*, 1986, **42**, 5459-5495.
2. M. C. Carreno, *Chem. Rev.*, 1995, **95**, 1717-1760.
3. E. N. Prilezhaeva, *Russ. Chem. Rev.*, 2001, **70**, 897-920.
4. G. K. S. Prakash, J. Hu and G. A. Olah, *J. Org. Chem.*, 2003, **68**, 4457-4463.
5. N. Fukuda and T. Ikemoto, *J. Org. Chem.*, 2010, **75**, 4629-4631.
6. V. Y. Kukushkin, *Coordination Chemistry Reviews*, 1995, **139**, 375-407.
7. M. Schuster, C. C. de Araujo, V. Atanasov, H. T. Andersen, K.-D. Kreuer and J. Maier, *Macromolecules*, 2009, **42**, 3129-3137.
8. I. Fernández and N. Khiar, *Chem. Rev.*, 2003, **103**, 3651-3706.
9. K. C. Lai, S. K. Lam, K. M. Chu, B. C. Y. Wong, W. M. Hui, W. H. C. Hu, G. K. K. Lau, W. M. Wong, M. F. Yuen, A. O. O. Chan, C. L. Lai and J. Wong, *N. Engl. J. Med.*, 2002, **346**, 2033-2038.
10. K. Kaczorowska, Z. Kolarska, K. Mitka and P. Kowalski, *Tetrahedron*, 2005, **61**, 8315-8327.
11. M. Focke, A. Feld and H. K. Lichtenthaler, *FEBS Lett.*, 1990, **261**, 106-108.
12. C. Pérez-Giraldo, G. Cruz-Villalón, R. Sánchez-Silos, R. Martínez-Rubio, M. T. Blanco and A. C. Gómez-García, *Journal of Applied Microbiology*, 2003, **95**, 709-711.
13. G. Merino, A. J. Molina, J. L. García, M. M. Pulido, J. G. Prieto and A. I. Alvarez, *Journal of Pharmacy and Pharmacology*, 2003, **55**, 757-764.
14. B. Kotelanski, R. J. Grozmann and J. N. Cohn, *Clin. Pharmacol. Ther.*, 1973, **14**, 427-433.
15. S. Padmanabhan, R. C. Lavin and G. J. Durant, *Tetrahedron Asym.*, 2000, **11**, 3455-3457.
16. J.-E. Baeckvall, 2010.

17. C.-Y. Chen, H. Zhang, L.-X. Zhang, L.-D. Li and Y.-L. Yan, *Youji Huaxue*, 2008, **28**, 1978-1981.
18. F. B. Souza and H. A. Stefani, 2014.
19. US20070203195A1, 2007.
20. H. Zhang, C. Chen, R. Liu, Q. Xu and W. Zhao, *Molecules*, 2010, **15**, 83-92.
21. H. Zhang, C.-Y. Chen, R.-H. Liu, Q. Xu and J.-H. Liu, *Synth. Commun.*, 2008, **38**, 4445-4451.
22. N. Baig, V. K. Madduluri and A. K. Sah, *RSC Adv.*, 2016, **6**, 28015-28022.
23. P. Pitchen and H. B. Kagan, *Tetrahedron Lett.*, 1984, **25**, 1049-1052.
24. R. S. Reddy, J. S. Reddy, R. Kumar and P. Kumar, *J. Chem. Soc., Chem. Commun.*, 1992, DOI: 10.1039/C39920000084, 84-85.
25. J. Legros and C. Bolm, *Chem. Eur. J.*, 2005, **11**, 1086-1092.
26. J. Legros and C. Bolm, *Angew. Chem. Int. Ed. (English)*, 2004, **43**, 4225-4228.
27. C. Drago, L. Caggiano and R. F. W. Jackson, *Angew. Chem. Int. Ed. (English)*, 2005, **44**, 7221-7223.
28. D. H. R. Barton, W. Li and J. A. Smith, *Tetrahedron Lett.*, 1998, **39**, 7055-7058.
29. M. Hirano, S. Yakabe, J. H. Clark and T. Morimoto, *J. Chem. Soc., Perkin Trans. 1 Journal of*, 1996, DOI: 10.1039/P19960002693, 2693-2698.
30. P. G. Cozzi, *Chem. Soc. Rev.*, 2004, **33**, 410-421.
31. M. De Rosa, M. Lamberti, C. Pellecchia, A. Scettri, R. Villano and A. Soriente, *Tetrahedron Lett.*, 2006, **47**, 7233-7235.
32. M. Palucki, P. Hanson and E. N. Jacobsen, *Tetrahedron Lett.*, 1992, **33**, 7111-7114.
33. Y. C. Jeong, S. Choi, Y. D. Hwang and K. H. Ahn, *Tetrahedron Lett.*, 2004, **45**, 9249-9252.
34. N. Y. Chen and W. E. Garwood, *J. Catal.*, 1978, **52**, 453-458.
35. S. Deshpande, D. Srinivas and P. Ratnasamy, *J. Catal.*, 1999, **188**, 261-269.
36. J. R. Anderson, K. Foger, T. Mole, R. A. Rajadhyaksha and J. V. Sanders, *J. Catal.*, 1979, **58**, 114-130.
37. M. R. Maurya, A. K. Chandrakar and S. Chand, *J. Mol. Catal. A: Chem.*, 2007, **274**, 192-201.
38. C. Jin, W. Fan, Y. Jia, B. Fan, J. Ma and R. Li, *J. Mol. Catal. A: Chem.*, 2006, **249**, 23-30.

39. K. J. Balkus and A. G. Gabrielov, in *Inclusion Chemistry with Zeolites: Nanoscale Materials by Design*, eds. N. Herron and D. R. Corbin, Springer Netherlands, Dordrecht, 1995, DOI: 10.1007/978-94-011-0119-6_6, pp. 159-184.
40. K. K. Bania and R. C. Deka, *J. Phys. Chem. C*, 2013, **117**, 11663-11678.
41. J. Zhu, Z. Kónya, V. F. Puntes, I. Kiricsi, C. X. Miao, J. W. Ager, A. P. Alivisatos and G. A. Somorjai, *Langmuir*, 2003, **19**, 4396-4401.
42. D. E. De Vos, M. Dams, B. F. Sels and P. A. Jacobs, *Chem. Rev.*, 2002, **102**, 3615-3640.
43. F. Bedioui, *Coord. Chem. Rev.*, 1995, **144**, 39-68.
44. K. N. Bhagya and V. Gayathri, *J. Porous Mater.*, 2013, **20**, 257-266.
45. S. Bunce, R. J. Cross, L. J. Farrugia, S. Kunchandy, L. L. Meason, K. W. Muir, M. O'Donnell, R. D. Peacock, D. Stirling and S. J. Teat, *Polyhedron*, 1998, **17**, 4179-4187.
46. H.-x. Feng, Y. Wang, R.-m. Wang and Y.-p. Wang, *Huaxue Shiji*, 2004, **26**, 1-2, 49.
47. I. Kuzniarska-Biernacka, K. Biernacki, A. L. Magalhaes, A. M. Fonseca and I. C. Neves, *J. Catal.*, 2011, **278**, 102-110.
48. M. R. Maurya, S. J. J. Titinchi and S. Chand, *J. Mol. Catal. A: Chem.*, 2003, **201**, 119-130.
49. IN192396A1, 2004.
50. D. Srinivas and S. Sivasanker, *Catal. Surv. Asia*, 2003, **7**, 121-132.
51. S. P. Varkey and C. R. Jacob, *Indian J. Chem., Sect. A: Inorg., Bio-inorg., Phys., Theor. Anal. Chem.*, 1999, **38A**, 320-324.
52. M. R. Maurya, M. Bisht and F. Avecilla, *J. Mol. Catal. A: Chem.*, 2011, **344**, 18-27.
53. M. R. Maurya, M. Bisht, N. Chaudhary, F. Avecilla, U. Kumar and H.-F. Hsu, *Polyhedron*, 2013, **54**, 180-188.
54. M. R. Maurya, P. Saini, C. Haldar and F. Avecilla, *Polyhedron*, 2012, **31**, 710-720.
55. M. R. Maurya, P. Saini, A. Kumar and J. Costa Pessoa, *Eur. J. Inorg. Chem.*, 2011, **2011**, 4846-4861.
56. F. Van de Velde, I. W. C. E. Arends and R. A. Sheldon, *Top. Catal.*, 2000, **13**, 259-265.
57. K. K. Bania, D. Bharali, B. Viswanathan and R. C. Deka, *Inorg. Chem*, 2012, **51**, 1657-1674.

58. M. Jafarian, M. Rashvand avei, M. Khakali, F. Gobal, S. Rayati and M. G. Mahjani, *J. Phys. Chem. C*, 2012, **116**, 18518-18532.

59. W. H. Quayle, G. Peeters, G. L. De Roy, E. F. Vansant and J. H. Lunsford, *Inorg. Chem*, 1982, **21**, 2226-2231.

60. W. H. Quayle and J. H. Lunsford, *Inorg. Chem.*, 1982, **21**, 97-103.

61. G. Ramanjaneya Reddy, S. Balasubramanian and K. Chennakesavulu, *J. Mater. Chem. A*, 2014, **2**, 15598-15610.

62. A. R. Silva, M. Martins, M. M. A. Freitas, A. Valente, C. Freire, B. de Castro and J. L. Figueiredo, *Microporous Mesoporous Mater.*, 2002, **55**, 275-284.

63. J. G. Dillard and L. T. Taylor, *J. Electron. Spectrosc. Relat. Phenom.*, 1974, **3**, 455-460.

64. L. J. Matienzo, W. E. Swartz and S. O. Grim, *Inorg. Nucl. Chem. Lett.*, 1972, **8**, 1085-1091.

65. J. C. Vedrine, M. Dufaux, C. Naccache and B. Imelik, *J. Chem. Soc. Faraday Trans.*, 1978, **74**, 440-449.

66. B. Dutta, S. Jana, R. Bera, P. K. Saha and S. Koner, *Appl. Catal., A*, 2007, **318**, 89-94.

67. R. Ganesan and B. Viswanathan, *J. Phys. Chem. B*, 2004, **108**, 7102-7114.

68. S. Deshpande, D. Srinivas and P. Ratnasamy, *Journal of Catalysis*, 1999, **188**, 261-269.

69. M. Khorshidifard, H. A. Rudbari, B. Askari, M. Sahihi, M. R. Farsani, F. Jalilian and G. Bruno, *Polyhedron*, 2015, **95**, 1-13.

70. M. M. Bhadbhade and D. Srinivas, *Inorg. Chem.*, 1993, **32**, 6122-6130.